

Raman scattering study of phonon and spin modes in (TMTSF)₂PF₆

Z. V. Popović^a, V. A. Ivanov^b, O. P. Khounk ^a, ,

T. Nakamura^c, G. Saito^d and V.V. Moshchalkov^a

^a *Laboratorium voor Vaste-Stoffysica en Magnetisme,*

K. U. Leuven, Celestijnenlaan 200D, B-3001 Leuven, Belgium

^b *Departement Natuurkunde, Universiteit Antwerpen UIA,*

Universiteitsplein 1, B-2610 Antwerpen, Belgium

^c *Research Institute for Electronic Science Hokudai University, Sapporo, 060-0812 Japan and*

^d *Department of Chemistry, Graduate School of Science,*

Kyoto University, Kyoto, 606-8501 Japan

Abstract

We have studied polarized Raman spectra of (TMTSF)₂PF₆ single crystals in the wide spectral and temperature range using different laser energies. We observed and assigned 23 Raman active modes. The carbon C=C in-phase and out-of-phase stretching modes at 1464 cm⁻¹ and 1602 cm⁻¹ show strong electron-molecular-vibration coupling. The mode at about 1565 cm⁻¹ is temperature independent below 50 K due to the methyl group motion freezing. For (TMTSF)₂PF₆ in the spin density wave phase for a temperature induced dimensionality 1D (quarter filled dimerized linear chain with correlated electrons) the spin gapless magnon spectra have been calculated. No evidence of spin-lattice coupling or spin-related modes is found in the Raman spectra in the spin density wave phase.

KEYWORDS: Organic superconductors, Raman spectroscopy, (TMTSF)₂PF₆, strongly correlated electrons, magnon dispersion.

PACS numbers: 78.30.Jw; 74.70.Kn; 75.30.Fv; 63.20.Dj;

I. INTRODUCTION

The $(\text{TMTSF})_2\text{PF}_6$ [bis-(tetramethyltetraselenafulvalene)hexafluorophosphate] salt is classified as a metal since it has metal-like conductivity almost in the whole temperature region except at very low temperatures. Due to the instability of the quasi-one-dimensional Fermi surface, at ambient pressure $(\text{TMTSF})_2\text{PF}_6$ undergoes a phase transition to a spin density wave (SDW) state below $T_{SDW} \simeq 12$ K. The SDW nesting is suppressed by applying pressure and this material becomes superconducting with $T_c = 1.1$ K, at $p = 6.5$ kbar [1]. Physical properties of this salt are discussed in details in Refs. [2, 3].

The $(\text{TMTSF})_2\text{PF}_6$ compound has a triclinic crystal structure [4] with $P\bar{1}$ space group and the unit cell parameters $a = 7.297$ Å, $b = 7.711$ Å, $c = 13.522$ Å, $\alpha = 83.39^\circ$, $\beta = 86.27^\circ$, $\gamma = 71.01^\circ$, $Z = 1$. Schematic representation of crystal structure in (ac) and (ab) plane is given in Figs. 1.(a) and 1.(b), respectively. As it can be seen from Fig. 1, the $(\text{TMTSF})_2\text{PF}_6$ crystal structure is dominated by stacks of the TMTSF molecules arranged in a zigzag pattern nearly perpendicular to the \mathbf{a} -axis [4]. The TMTSF molecules appear to be weakly dimerized by their actual position in the unit cell. By lowering the temperature the triclinic stabilization becomes even stronger, as stated in Ref.[5].

In spite of the intense research efforts the superconducting state in $(\text{TMTSF})_2\text{PF}_6$ and other isostructural $(\text{TMTSF})_2\text{X}$ ($\text{X} =$ monovalent anion like ClO_4^- , FSO_3^- , PF_6^- or AsF_6^-) Bechgaard salts is not yet fully understood. It should be also mentioned that these materials have attracted more attention in the last years because of the normal state, *i.e.* that of a quasi-one-dimensional metal, and because of the SDW state [6, 7, 8, 9, 10, 11]. Below T_{SDW} the presence of antiferromagnetic ordering is confirmed by both ESR [12] and NMR [13] measurements. The spin-density-wave gap of $(\text{TMTSF})_2\text{PF}_6$ at about $\Delta = 4.5$ meV (35 cm^{-1}) is obtained from the far-infrared reflectivity measurements using the E||b' polarized light [9]. The electron tunneling spectroscopy revealed even smaller value of the SDW gap: 2.5-2.9 meV [14], which is consistent with the one obtained by the infrared absorption, $\Delta = 2.5$ -4.3 meV [15].

Phonon properties of $(\text{TMTSF})_2\text{PF}_6$ were poorly studied because the phonons are masked by the free carriers (plasmons) in the infrared and the far-infrared spectral regions. On the other hand, an extremely low scattering efficiency and temperature instability of $(\text{TMTSF})_2\text{PF}_6$ hindered Raman scattering measurements. Because of that, only the vibra-

tional properties of the TMTSF neutral molecule and its radical cation were studied in more details [16] by the infrared and Raman spectroscopies and the normal coordinate analysis based on a modified valence force field (VFF) model. The Raman scattering in organic superconductors is not widely used because of a very weak intensity of the Raman signal. The most studied organic superconductors by the Raman spectroscopy are κ -(BEDF-TTF)₂X salts [17, 18, 19]. To the best of our knowledge the Raman spectra of (TMTSF)₂PF₆ were measured only in Ref.[20, 21]. Iwahana *et al.* found two well shaped modes at 1463 cm⁻¹ and 1559 cm⁻¹ (see Fig. 2 of Ref. [20]). All other modes had the intensity comparable with the level of noise. Krauman *et al.* shown that the intensity of the Raman modes of (TMTSF)₂PF₆ is strongly enhanced with 647.1 nm line of Kr laser [21].

In this paper we present the polarized Raman spectra of the (TMTSF)₂PF₆ single crystals measured with different laser excitation energies in the wide spectral and temperature range ($4K < T < 300K$). Totally 23 Raman active modes are observed, including 6 reported for the first time. The C=C in-phase and out-of-phase stretching modes at 1464 and 1602 cm⁻¹ show an equal frequency shift from both the neutral (TMTSF)⁰ molecule and its radical cation (TMTSF)⁺ as a consequence of quarter filling. The mode at about 1565 cm⁻¹, which represents the CH₃ methyl group motion, shows no frequency shift at temperatures below 50 K because of vibrations freezing of CH₃ molecule. We calculated the magnon dispersion for the dimerized quarter-filled antiferromagnetic linear chains and did not find the spin-gapped state in the SDW phase. The Raman spectra in the SDW state ($4K < T < 12K$) shown no evidence of spin-related features.

II. EXPERIMENTAL DETAILS

The single crystals of the (TMTSF)₂PF₆ have been prepared by the electrocrystallization method [22]. The samples have a needle-shaped form with typical dimensions 2 mm x 0.5 mm x 0.05 mm along the **a**, **b'** and **c'**- axis, respectively. The Raman spectra were recorded in the backscattering configuration using micro-Raman system with Dilor triple monochromator including liquid nitrogen cooled CCD-detector. For low-temperature measurements we used Oxford Microstat^{He} continuous flow cryostat with 0.5 mm thick window. Focusing of the laser beam was realized with long distance (10 mm focal length) microscope objective (magnification 50X). As an excitation source we used an Ar-ion laser. Overheating of the

samples was observed with the laser power levels as low as 10 mW (0.6 mW at the sample). We found that laser power level of 0.02 mW on the sample is sufficient to obtain Raman signal and, except for the signal-to-noise ratios, no changes of the spectra were observed as a consequence of laser heating by further lowering of laser power. Corresponding excitation power density was less than 0.1 kW/cm².

III. EXPERIMENTAL RESULTS

Figure 2 shows the (aa) polarized low temperature (T=10 K) Raman spectra of (TMTSF)₂PF₆ in the 1300 - 1700 cm⁻¹ spectral region, excited with 457.9 nm (a) and 514.5 nm (b) energies. The main difference between these spectra is an intensity enhancement of 1565 cm⁻¹ (1602 cm⁻¹) mode with 457.9 nm (514.5 nm) excitation, as a result of the resonance effect. Figure 3 shows (b'b') polarized Raman spectrum of (TMTSF)₂PF₆ measured at 10 K in the spectral range from 150 to 1700 cm⁻¹. The same spectra in the 2700-3000 cm⁻¹ range is given in the inset of Fig. 3. Further lowering of temperature up to our experimental limit of 4 K does not produce any change in the Raman spectra. As we expected, we have got better signal to noise ratio for (b'b') polarization (b'=insulating axis) than in the (aa) case. We observed 23 Raman active modes in four spectral ranges: (i) 2800 - 3000 cm⁻¹; (ii) 1450 - 1650 cm⁻¹; (iii) 900 - 1100 cm⁻¹ and (iv) below 500 cm⁻¹. As we will discuss in the next Section, the highest frequency modes originate from the CH₃ methyl group vibrations, the strongest intensity modes in the second range represent in-phase and out-of-phase bond stretching C=C vibrations; the C-C-H bending vibrations are localized in the third spectral range and the bond stretching C-Se and Se-Se vibrations have energies lower than 500 cm⁻¹. The lowest energy modes (below 200 cm⁻¹) correspond to the rotational motion of TMTSF molecules. The influence of temperature and laser power on Raman spectra in the 1300-1700 cm⁻¹ spectral range is illustrated in Figure 4. Figure 5 shows the full width at half maximum (FWHM) and the frequency vs. temperature dependencies of the C=C in phase stretching mode.

IV. DISCUSSION

A. Normal state

The unit cell of $(\text{TMTSF})_2\text{PF}_6$ ($[(\text{CH}_3)_4\text{C}_6\text{Se}_4]_2\text{PF}_6$) consists of one formula unit with 59 atoms in all. Since there is a large number of atoms in the unit cell, we can expect a very large number of optically active modes. All atoms (except P-atom which is in (a) position-center of inversion) have 2(i) position symmetry (C_1) of $P\bar{1}$ space group [4]. Factor-group-analysis (FGA) yields:

$$\text{C, Se, H, F } (C_1): \Gamma = 3A_g + 3A_u$$

$$\text{P } (C_i): \Gamma = 3A_u$$

Summarizing these representations we obtain the irreducible representations of $(\text{TMTSF})_2\text{PF}_6$ vibrational modes:

$$\Gamma_{P\bar{1}} = 87A_g + 90A_u \tag{1}$$

According to this representation one can expect 177 modes from which 87 are Raman active. Experimentally, the number of observed modes is less than 25. The missing modes are not seen since their intensity is probably below the noise level of our measurements.

Let us consider first the properties of each molecule in $(\text{TMTSF})_2\text{PF}_6$, separately. Three modes were observed in the Raman spectra of hexafluorophosphate (PF_6^-) in different inorganic compounds [23]. The strongest mode appears at about 750 cm^{-1} and two other modes at about 575 cm^{-1} (the intensity of this mode is 12% of the strongest mode intensity) and at 475 cm^{-1} (20%). We did not find any evidence of 750 cm^{-1} and 575 cm^{-1} PF_6^- Raman modes in Raman spectra of $(\text{TMTSF})_2\text{PF}_6$ (see Fig. 3). At about 475 cm^{-1} one mode exists, but, because we did not find the strongest intensity mode of PF_6^- , we concluded that this mode belongs to the TMTSF molecule. Thus, the Raman spectra of $(\text{TMTSF})_2\text{PF}_6$ can be considered by comparison only with corresponding spectra of the TMTSF molecule. Vibrational properties of the TMTSF neutral molecule and its radical cation TMTSF^+ have been subject of experimental and theoretical studies in Refs. [16, 20, 21]. We used these results to assign our spectra, Table I. Last column in Table I shows the assignment of the observed modes obtained using normal coordinate analysis based on the valence-force-field (VFF) model [16]. As it is shown in Table I, our results are in a very good agreement with

the previously published data. Beside that, we observed 6 new modes in $(\text{TMTSF})_2\text{PF}_6$ for the first time. Because the carriers (holes) are located in the central part of the TMTSF molecule (C_2Se_4 fragment) we have paid special attention to spectral region below 500 cm^{-1} (C-Se and Se-Se vibration, see normal coordinates ν_{10} and ν_{11} of these modes, Fig.1(a)) and between 1400 and 1700 cm^{-1} ($\nu_4=1464\text{ cm}^{-1}$ mode, in-phase C=C stretching and $\nu_3=1602\text{ cm}^{-1}$ mode, out-of-phase C=C stretching). Contrary to Ref. [16], we found that ν_{11} mode at 263 cm^{-1} (Se-Se stretching) exists both in the $(\text{TMTSF})_2\text{PF}_6$ and in the neutral TMTSF^0 molecule. Also, 284 cm^{-1} mode (ν_{10} , Se-C stretching) appears in $(\text{TMTSF})_2\text{PF}_6$ and in an ion TMTSF^+ at the same frequency. It was reported in Ref. [16] that these modes, due to ionization, have huge positive frequency shifts ($+41\text{ cm}^{-1}$ (ν_{10}), $+22\text{ cm}^{-1}$ (ν_{11})) from neutral molecule to the TMTSF^+ ion. We have revealed that no frequency shift exists for these two modes, and consequently these modes show negligible coupling with charge carriers.

A remarkable negative frequency shift is found for the C=C vibrational modes. The ν_4 mode frequency shift of about -70 cm^{-1} (-140 cm^{-1}) is observed between the neutral TMTSF^0 molecule and the $(\text{TMTSF})_2\text{PF}_6$ (TMTSF^+ ion). The ν_3 mode shows also negative shift of about -23 cm^{-1} between TMTSF^0 and $(\text{TMTSF})_2\text{PF}_6$. The observed frequency shift is a consequence of the coupling between charge, located at the central fragment of the molecules, and the C=C stretching A_g vibrations (arising due to the electron-molecular-vibration (EMV) coupling) [24]. As stated in [18], these two modes have the strongest EMV coupling constants among all observed modes in the TMTSF salts. It is interesting to note that a negative frequency shift of the C=C modes between the neutral TMTSF molecule and the same molecule in $(\text{TMTSF})_2\text{PF}_6$ *is exactly twice less than the same frequency shift between the neutral TMTSF molecule and its radical ion, as a consequence of quarter-filling.*

In Fig. 4(a)-(f) we present the Raman spectra of $(\text{TMTSF})_2\text{PF}_6$ measured for the (b'b') polarization at different temperatures in the $1300 - 1700\text{ cm}^{-1}$ range. Spectrum in Fig. 4(f) is observed at 10 K but with an increased excitation power by a factor of 12 in comparison with the 10 K measurements shown in Fig. 4(e). Frequency shift of this mode of about 3 cm^{-1} to lower energy and mode broadening ($\text{FWHM}=7.5\text{ cm}^{-1}$) are clear indications of the sample heating. In order to analyze the frequency vs. temperature dependence of high intensity modes we measured the Raman spectra for the (b'b') polarization in the wide temperature range with very low excitation level ($<0.1\text{ kW/cm}^2$). The frequency and FWHM vs temperature dependencies of 1464 cm^{-1} mode are given in Fig. 5. The same kind

of temperature dependence is found for the second C=C mode (ν_3). As it is shown in Fig. 5(b) the frequency of the C=C mode has a parabolic decrease with temperature. We found that this dependence can be described as $\omega(\text{cm}^{-1}) = 1464.3 - 5.5 \times 10^{-3}T - 48 \times 10^{-6}T^2$, where T is a temperature in K. Using these data (Fig. 5) we estimated the actual temperature of the sample in the spectra from Fig. 4(f) as 225 K. The mode at about 1565 cm^{-1} shows a stronger frequency vs. temperature dependence by lowering temperature from 300 to 50 K than the C=C modes. Because the frequency of this mode does not change below 50 K (see the right panel of Fig. 4), we concluded that this mode originates from the H-C-H bending vibrations. As proposed in Ref. [13] dealing with the NMR data, the motion of methyl group is frozen at about 50 K, fully in an agreement with our findings.

B. Spin-density-wave state

Discussion of the magnon or spin gap excitations in quasi-one-dimensional chains is questionable without the theoretical calculation of the magnon dispersion. Namely, it is well known that the non-dimerized Heisenberg chain with antiferromagnetically coupled localized 1/2 spins does not have spin-gap. To the best of our knowledge there are no magnon dispersion calculations for a quarter-filled dimerized chain with correlated electrons, the case under consideration here.

In order to calculate magnon dispersion we started from the $(\text{TMTSF})_2\text{X}$ Hamiltonian [25] in the form:

$$\begin{aligned} \mathcal{H} = & -t_1 \sum_{i \text{ even}, l, \sigma} \left(c_{i,l,\sigma}^+ c_{i+1,l,\sigma} + H.c. \right) - t_2 \sum_{i \text{ odd}, l, \sigma} \left(c_{i,l,\sigma}^+ c_{i+1,l,\sigma} + H.c. \right) \\ & - t_b \sum_{i,l,\sigma} \left(c_{i,l,\sigma}^+ c_{i,l+1,\sigma} + H.c. \right) + U \sum_{i,l} c_{i,l,\uparrow}^+ c_{i,l,\uparrow} c_{i,l,\downarrow}^+ c_{i,l,\downarrow}. \end{aligned} \quad (2)$$

Here $t_{1,2}$ and t_b are alternating hopping energies along the chain (indices l and i denote chains and chain sites, respectively), and along b-axis, respectively (Fig.1(b)) and U is on-site Coulomb repulsion. According to the quantum chemical calculations [26] and spectroscopy data for the TMTSF molecule, the charge density profile of the hole is located around the central fragment C_2Se_4 . The Se $4s$ and $4p$ orbitals contribute to the conduction bands with a density such as one hole (or three electrons) per $(\text{TMTSF})_2$ dimer (unit cell). Furtheron we will use the hole representation. The charge localization at the centers of the TMTSF molecules and a small overlap of the molecular orbitals in solid means that carriers prefer to

stay at the TMTSF sites than to move. This leads to an enhancement of the intraTMTSF Coulomb repulsion (the Anderson-Hubbard parameter U) of carriers and to the narrowness of energy bands in the $(\text{TMTSF})_2\text{PF}_6$ compound. For the κ -BEDT-TTF₂X salts with the central fragment C₂S₄ the recent estimations [27, 28] have shown that the U values ($U=3.56$ eV - 4.21 eV [28] or even $U=5.37$ eV [27]) are extremely high with respect to the hopping energy $t \sim 0.1$ eV. We can assume that in the TMTSF molecule $U=4$ eV. This value can be estimated from the atomic energy 1Ry (characteristic electron correlation energy for light atoms with size 1Å) multiplied by the ratio of this size (around 1Å) to the size of the C₂Se₄ fragment (3.5Å).

In Eq.(2), the hopping Hamiltonian is diagonalized in the standard way and the carrier energy dispersions are given by $\varepsilon_p^\pm = -2t_b \cos p_x \pm \sqrt{t_1^2 + t_2^2 + 2t_1 t_2 \cos p_y}$ leading to non-correlated anisotropic band structure. The dimerization band gap between the bonding and antibonding non-correlated bands is $\Delta_d = 2(|t_1 - t_2| - 2t_b)$.

Due to the on-site electron interaction U , for TMTSF one can carry out the mapping of the Hamiltonian, Eq. (2), to the projected X-operators [29, 30] such as $c_\sigma = X^{0\sigma} + \sigma X^{\bar{0}\bar{\sigma}}$. The tight-binding method for correlated electrons has been shortly presented by us earlier for study of the transition metal oxides, high- T_c cuprates, organic materials, spin-ladders (see [31, 32, 33, 34, 35] and Refs. there).

In Raman scattering measurements the heating of the sample due to laser irradiation induces thermal fluctuations which can destroy the coherent interchain hopping amplitude and reduce the dimensionality of $(\text{TMTSF})_2\text{PF}_6$ to 1D. The temperature induced dimensional crossover has been revealed by transport properties [6], a microwave conductivity [36] and a specific heat [37] measurements. According to these investigations the crossover temperature T' varies in the range 3 K-35 K. The theoretical estimations give even smaller magnitudes of T' . In the $(\text{TMTSF})_2\text{PF}_6$ model as weakly coupled Luttinger chains $T' \sim (t_b/t_a^\alpha)^{1/(1-\alpha)}(t_a = t_1 = t_2)$ with $\alpha = (K_\rho + 1/K_\rho - 2)/4$ [38], and values of K_ρ in the range 0.2-0.25 or 0.35 [39]. In contrast, the recent Hall effect and electrical conductivity measurements [6] in $(\text{TMTSF})_2\text{PF}_6$ confirm the Fermi-liquid description at $T \lesssim 300\text{K}$ with the possible 1D Luttinger liquid picture well above room temperature. At the assumption that in our experiment we are dealing with $T > T'$, in the range of temperature reduced dimensionality, the minimal model for $(\text{TMTSF})_2\text{PF}_6$ salt is the dimerized quarter-filled linear chain with correlated electrons ($t_b=0$).

To calculate the magnon energy dispersions in SDW-state in TMTSF-chain, first of all we split the lattice into two sublattices, a and b , with opposite spins. In sublattice $a(b)$ with spin projection up (down) the localized magnon (zeroth order approximation) has energy $\omega_{+-} = \varepsilon_- - \varepsilon_+ = 2H$ ($\omega_{-+} = \varepsilon_+ - \varepsilon_- = -2H$, the Bohr magneton $\mu_B = 1$) in magnetic field H . In the second order of the perturbation theory the inverse magnon Green's function is presented by the two-by-two matrix as follows:

$$D_{+-}^{-1}(p, \omega) = \begin{matrix} +- \\ -+ \end{matrix} \begin{pmatrix} \frac{-i\omega}{f_{+-}^a} + 2H + \Pi_{aa} & \Pi_{ab} \\ \Pi_{ba} & \frac{i\omega}{f_{-+}^b} - 2H + \Pi_{bb} \end{pmatrix}. \quad (3)$$

In Eq.(3) the diagonal, $\Pi_{aa,bb}$, and non-diagonal, $\Pi_{ab,ba}$, magnon self-energies (polarization operators) are defined by the sum of diagrams presented in Figure 6. For a quarter filled chain the magnon correlation factors are defined as $f_{\sigma\bar{\sigma}} = n_\sigma - n_{\bar{\sigma}} = n_\sigma = \frac{1}{2}$. Each polarization diagram includes a pair of hole hops between sublattices. The internal solid lines are the hole Green's functions $G_\alpha^{a,b}(q, \omega) = 1/(-i\omega_n + \xi_q - \mu)$, with correlated energies $\xi_q = \frac{U}{2} \pm \frac{1}{2} \sqrt{U^2 + 4f_a^{0+} f_b^{2-} \varepsilon_q^2}$, where ε_q is the non-correlated tight-binding dispersion, μ is the chemical potential and $f_{a,b}^{0+,2-}$ are the fermionic correlation factors (Fig.6). In paramagnetic phase the correlation factors are governed by a carrier concentration. In each sublattice the spin ordered electrons can be considered as spinless fermions, for which the fermionic correlation factors $f_{a,b}^\alpha = 1$

The diagonal magnon-self energies (Fig. 6(a)) are momenta independent and have analytical expressions such as

$$\Pi_{aa,bb} = -4 \frac{t_1^2 + t_2^2}{U}. \quad (4)$$

For small difference between hopping integrals along slightly dimerized chains, $|t_1 - t_2| \ll U$, of the (TMTSF)₂PF₆ salt (the existing evaluations for hopping energies are $t_1=147$ meV [40], 252 meV [41] and $t_2=144$ meV [40], 209 meV [41]) the non-diagonal self-energies, Π_{ab} and Π_{ba} are momenta dependent and composed from diagrams in Figs. 6(b), 6(c), which can be expressed analytically as follows

$$\Pi_{ab} = \frac{4}{U}(t_1^2 + t_2^2 e^{2ip}) + o\left(\frac{t_1^2 - t_2^2}{U}\right), \quad \Pi_{ba} = \frac{4}{U}(t_1^2 + t_2^2 e^{-2ip}) + o\left(\frac{t_1^2 - t_2^2}{U}\right). \quad (5)$$

After an analytical continuation, $i\omega \rightarrow \omega + i\delta$ and putting $H \rightarrow 0$, the zeros of the inverse magnon Green's function, Eq. (3), (poles of the Green's function $D_{+-}(p, \omega)$) give the spin-wave spectrum

$$\omega(p) = 2n_\sigma \frac{4t_1 t_2}{U} \sin p = \frac{4t_1 t_2}{U} \sin p, \quad (6)$$

for a considered model of the (TMTSF)₂PF₆ salts with one carrier per dimer (TMTSF)₂ ($n = 1$, $n_\sigma = 1/2$).

It is important to note that in the limiting case of a half-filled nondimerized chain ($n=2$, $n_\sigma=1$, $t_1 = t_2 = t$) the Eq.(6) gives the conventional gapless spectrum of spin-waves as $\omega(p) = 2J \sin p$ with exchange parameter $J = 4t^2/U$. In this case the magnon amplitude is higher *by factor $4/\pi$ only*, than exact the des Clozeaux-Pearson result for spins 1/2 in the Heisenberg chain, $\frac{\pi}{2} J \sin p$ [42, 43].

In Raman spectra at 4 K we found no difference with the corresponding spectra above 10-12 K. This has to be expected because:

(i) It was reported [44] that the spin-lattice coupling in the SDW state is very weak in (TMTSF)₂PF₆, and consequently the phonon frequency shift at SDW transition is not observable. Also, the heat capacity does not change significantly at T_{SDW} [45].

(ii) Raman scattering due to magnetic excitation is usually very weak in low-dimensional systems. Because of a weak antiferromagnetic ordering in (TMTSF)₂PF₆ it is hard to expect an appearance of new spin-related modes. Effect of magnetic fluctuations on Raman scattering was analyzed only in the κ -BEDT-TTF₂Cu(NCS)₂ organic superconductor [19]. It was shown that the frequencies of two modes soften in the temperature range where antiferromagnetic spin fluctuations (80 K) have been observed. In our case the critical temperature (12 K) is too close to our experimental limit (4K) and no frequency shift is observed.

(iii) For TMTSF salts Yamaji predicted [46] that a phase transition from metallic to SDW state occurs in two steps. At T_{SDW} , there is a transition, first from metallic into semimetallic SDW state and after that at $T^* < T_{SDW}$ into an insulating SDW state. Such picture in (TMTSF)₂PF₆ is verified by transport measurements [47, 48, 49] under pressure and/or in high magnetic fields [50, 51, 52]. Furthermore, the proton NMR measurements [53] have shown no nuclei damping below $T^* \simeq 3.5$ K and the Korringa-like ⁷⁷Se spin lattice relaxation rate has been found between T^* and T_{SDW} [54], with activated character below $T^* \simeq 4$ K. Thus, the coexistence of metallic and SDW states above T^* leads to an incomplete SDW gap and also hinders an observation of the spin modes in Raman spectra.

(iv) Finally, we can not totally exclude the effect of the sample heating by laser irradiation,

which can destroy the coherent interchain hopping amplitude and reduce the dimensionality of $(\text{TMTSF})_2\text{PF}_6$ to 1D.

In conclusion, we have measured the polarized Raman spectra of $(\text{TMTSF})_2\text{PF}_6$ single crystals in a wide spectral and temperature range using different laser energies. We observed and assigned 23 Raman active modes, of which 6 are observed for the first time. We found that Se-Se and C-Se stretching modes at 263 cm^{-1} and 284 cm^{-1} , respectively do not have a positive frequency shift in comparison with corresponding modes of (TMTSF) neutral and ionized molecule, i.e. these modes are not coupled with charge carriers. Only the C=C stretching modes at about 1464 and 1602 cm^{-1} show the strong electron-molecular-vibration coupling. We found that the frequency vs temperature dependence of the strongest intensity mode is $\omega(\text{cm}^{-1}) = 1464.3 - 5.5 \times 10^{-3}T - 48 \times 10^{-6}T^2$, where T is a temperature in K. The mode at about 1565 cm^{-1} shows no temperature shift below 50 K due to the CH_3 methyl group motion freezing.

We calculated magnon dispersion for the one-dimensional correlated quarter-filled chains for the first time. Our calculation for a temperature reduced 1D and slightly dimerized $(\text{TMTSF})_2\text{PF}_6$ salt in the SDW phase does not show the spin gap at quarter-filling. We found no difference in the Raman spectra between the normal and the SDW state as a consequence of a very weak antiferromagnetic ordering in the SDW phase or possibly due to an imperfect SDW phase in the temperature range $4\text{ K} < T < 12\text{ K}$.

Acknowledgment

Z.V.P., V.A.I and O.P.K acknowledge support from the Research Council of the K.U. Leuven and DWTC. The work is supported by the ESF Program FERLIN and the Belgian IUAP and FWO-VI and GOA Programs. V.A.I. acknowledges illuminating discussions with K. Yamaji about the $(\text{TMTCF})_2\text{X}$ phase diagram and with Yu. Kagan.

-
- [1] D. Jérôme, A. Mazaud, M. Ribault, and K. Bechgaard, *J. Physique Lett.*, **41**, L95 (1980).
- [2] T. Ishiguro, K. Yamaji, and G. Saito, *Organic Superconductors*, Springer Series in Solid-State Sciences, Vol. 88 (Springer, Berlin, 1998) and Refs. there.
- [3] L. P. Gor'kov, *J. Phys. I (France)*, **6**, 1697 (1996).
- [4] N. Thorup, G. Rindorf, H. Soling, and K. Bechgaard, *Acta Crys. B* **37**, 1236 (1981);
- [5] K. Bechgaard, M. M. Nielsen and F. C. Krebs, *J. Phys. IV (France)* **10**, Pr3-11, (2000).
- [6] G. Mihály, I. Kézsmárki, F. Zámorszky and L. Forró, *Phys. Rev. Lett.* **84** 2670 (2000).
- [7] J. Moser, J. R. Cooper, D. Jérôme, B. Alavi, S. E. Brown and K. Bechgaard, *Phys. Rev. Lett.* **84**, 2674 (2000).
- [8] M. Dressel, *Physica C* **317-318**, 89 (1999).
- [9] L. Degiorgi, M. Dressel, A. Schwartz, B. Alavi and G. Grüner, *Phys. Rev. Lett.* **76**, 3838 (1996).
- [10] V. Vescoli, L. Degiorgi, W. Henderson, G. Grüner, K. P. Starkey, and L. K. Montgomery, *Science* **281**, 1181 (1998).
- [11] S. Zherlitsyn, G. Bruls, A. Goltsev, B. Alavi and M. Dressel, *Phys. Rev. B* **59**, 13861 (1999).
- [12] W. M. Walsh Jr., F. Wudl, G. A. Thomas, D. Nelewajek, J. J. Hauser, P. A. Lee, and T. Poehler, *Phys. Rev. Lett.* **45**, 829 (1980).
- [13] J. C. Scott, H. J. Pedersen, and K. Bechgaard, *Phys. Rev. B* **24**, 475 (1981).
- [14] K. Ichimura, O. Abe, K. Nomura, S. Takasaki, J. Yamada, S. Nakatuiji, and H. Aazai, *Synth. Metals*, **103**, 2097 (1999).
- [15] K. Kornelsen, J.E. Ebbbridge, G.S.Bates, *Phys. Rev. B* **55**, 9162 (1987).
- [16] M. Meneghetti, R. Bozio, I. Zanon, C. Pecile, and C. Ricotta, *J. Chem. Phys.* **80**, 6210 (1984).
- [17] S. Sugai, H. Mori, H. Yamochi and G. Saito, *Phys. Rev. B* **47**, 14374 (1993).
- [18] D. Pedron, G. Visentini, E. Cecchetto, R. Bazio, J. M. Williams and A. Schlueter, *Synth. Metals*, **85**, 1509, (1997).
- [19] Y. Lin, J. E. Eldridge, H. H. Wang, A. M. Kini, M. E. Kelly, J. M. Williams and J. Schlueter, *Phys. Rev. B* **58**, R599 (1998).
- [20] K. Iwahana, H. Kuzmany, F. Wudl, E. Aharon-Shalom, *Mol. Cryst. Liq. Cryst.*, **79**, 39 (1982).
- [21] M. Krauzman, H. Poulet, and R. M. Pick, *Phys. Rev. B* **33**, 99 (1986).

- [22] Ref[2], p.448
- [23] R. A. Niquist, C. L. Putzig, M. A. Leugers, *The Handbook of Infrared and Raman Spectra of Inorganic Compounds and Organic Salts*, Academic Press, New York, 1996, p.19.
- [24] M. J. Rice, *Solid State Commun.*, **31**, 93 (1979).
- [25] V. A. Ivanov and K. Yamaji, unpublished.
- [26] R. V. Metzger, *J. Chem. Phys.* **75**, 482 (1981).
- [27] Y. Okuno and H. Fukutome, *Solid State Commun.* **101**, 355 (1997).
- [28] A. Fortunelli and A. Painelli, *Phys. Rev. B* **55**, 16088 (1997).
- [29] S. Okubo, *Prog. Theor. Phys.*, **27**, 949 (1962).
- [30] J. Hubbard, *Proc Roy. Soc. A* **276**, 238 (1963), *ibid.* **277**, 237 (1964).
- [31] V. A. Ivanov, *Physica B* **186-188**, 921 (1993).
- [32] V. A. Ivanov, *J. Phys. Condens. Matter*, **6**, 2065(1994); *Physica C*, **185-189**, 1635 (1991).
- [33] V. A. Ivanov, E. A. Ugolkova, and M. Ye. Zhuravlev, *Sov. Phys. JETP* **86**, 395 (1998).
- [34] Z. V. Popović, M. J. Konstantinović, V. A. Ivanov, O. P. Khuong, R. Gajić, A. Vietkin and V. V. Moshchalkov, *Phys. Rev. B* **62**, 4963 (2000).
- [35] V. A. Ivanov, Z. V. Popović, O. P. Khuong, and V. V. Moshchalkov, cond-mat/9909046.
- [36] P. Fertey, M. Poirier, and P. Batial, *Synth. Metals*, **103**, 2076 (1999).
- [37] J. C. Lazjaunias, K. Biljaković, H. Yang, and P. Monceau, *Synth. Metals*, **103**, 2130 (1999).
- [38] C. Bourbonnais, *J. Phys. IV (France)*, **10**, 3 (2000).
- [39] A. Georges, T. Giamazcki and N. Sandler, cond-mat/0001063.
- [40] P. M. Grant, *Phys. Rev. B* **26**, 6888 (1982).
- [41] L. Ducasse, M. Abderrabba, J. Hoarau, M. Pesquer, B. Gallois and J. Gaultier, *J. Phys. C* **19**, 3805 (1989).
- [42] J. des Clozeaux and J. J. Pearson, *Phys. Rev.* **128**, 2131 (1962).
- [43] A. A. Ovchinnikov, *Sov. Phys. JETP*, **29**, 727 (1969).
- [44] G. Kreuzet, C. Gaonach and B. Hamzić, *Synth. Metals*, **19**, 245 (1987).
- [45] J. Coroneus, B. Alavi, S. E. Braun, *Phys. Rev. Lett.*, **70**, 2332 (1993).
- [46] K. Yamaji, *J. Phys. Soc. Japan*, **51**, 2787 (1982); also Ref.[2], p.102.
- [47] J. P. Ulmet, P. Auban, A. Khmou, S. Askenazy, and A. Moradpour, *J. Phys. Lett.(Paris)*, **46**, 535 (1985).
- [48] S. Uji, J. S. Brooks, M. Chaparala, S. Takasaki, J. Yamada and H. Anzai, *Phys. Rev. B* **55**,

- 12446 (1997).
- [49] J. S. Brooks, J. O'Brien, R. P. Starrett, R. G. Clark, R. H. McKenzie, S. Y. Han, J. S. Qualls, S. Takasaki, J. Yamada, H. Anzai, and L. K. Montgomery, *Phys. Rev. B* **59**, 2604 (1999).
 - [50] A. Audouard and S. Ashkenazy, *Phys. Rev. B* **52**, 700 (1995).
 - [51] N. Biškup, S. Tomić, D. Jérôme, *Phys. Rev. B* **51**, 11972 (1995).
 - [52] K. Maki, *Phys. Rev. B* **47**, 11506 (1993).
 - [53] T. Takahashi, T. Harada, Y. Kobayashi, K. Kanoda, K. Suzuki, K. Murata, and G. Saito, *Synth. Metals*, **41-43**, 107 (1985).
 - [54] S. Valfells, R. Kuhns, A. Kleinhammes, J. S. Brooks, W. Moulton, S. Takasaki, J. Yamada, and H. Anzai, *Phys. Rev. B* **56**, 2585 (1997).

FIG. 1: Schematic representation of the $(\text{TMTSF})_2\text{PF}_6$ crystal structure in the (a) (010) and (b) (001) plane. The dashed lines represent the unit cell.

FIG. 2: Raman scattering spectra of $(\text{TMTSF})_2\text{PF}_6$ for the (aa) polarization at 10 K.

FIG. 3: Raman scattering spectra of $(\text{TMTSF})_2\text{PF}_6$ for the (b'b') polarization at 10 K.

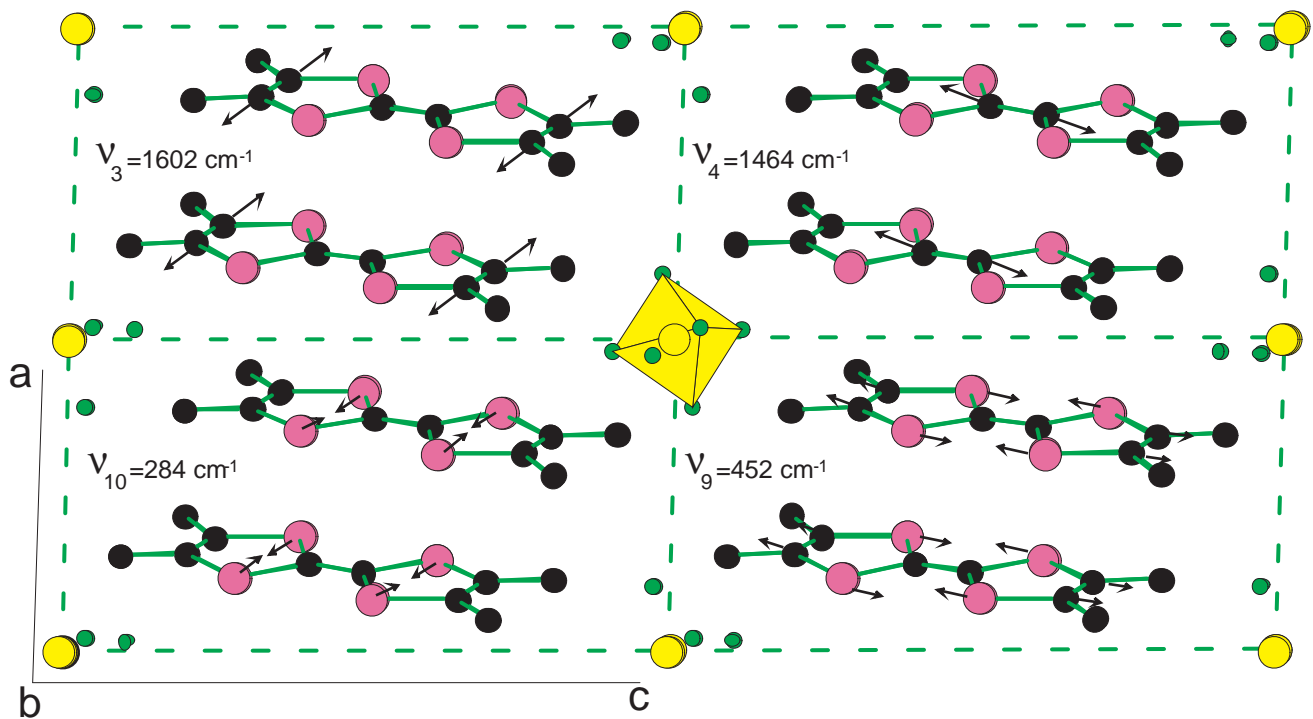
FIG. 4: Raman scattering spectra of $(\text{TMTSF})_2\text{PF}_6$ for the (b'b') polarization at different temperatures and laser power: (a)-(e) $P=0.1 \text{ kW/cm}^2$, (f) $P=1.2 \text{ kW/cm}^2$.

FIG. 5: Frequency and FWHM vs temperature dependencies of the 1464 cm^{-1} mode. The solid line is parabolic fit $\omega(\text{cm}^{-1}) = 1464.3 - 5.5 \times 10^{-3}T - 48 \times 10^{-6}T^2$.

FIG. 6: The second order polarization operator diagrams for "diagonal", $\Pi_{aa,bb}$, and "non-diagonal", $\Pi_{ab,ba}$, magnon self-energies in Eq.(3). Solid lines denote magnon (+-, -+) and fermion (α, β) Green's functions, whereas dashed lines ("interactions") mark the hole hopping energies between sublattices of dimerized TMTSF-chain. The "triangular" arrows stand for the on-site transitions labeled by $su(2, 2)$ superalgebra roots α, β . The circles stand for fermionic correlation factors $f^{pq} = \langle X^{pp} + X^{qq} \rangle_0$. (a) For Π_{aa} (left diagram) the on-site transitions are labeled by roots $\alpha = 2 - (0-)$ and $\beta = +0(+2)$. For Π_{bb} (right diagram) the on-site transitions are labeled by roots $\alpha = 0 + (2+)$ and $\beta = -2(-0)$. (b) Polarization diagrams for the self energy $\Pi_{ab}(p)$. (c) Polarization diagrams for the self-energy $\Pi_{ba}(p)$.

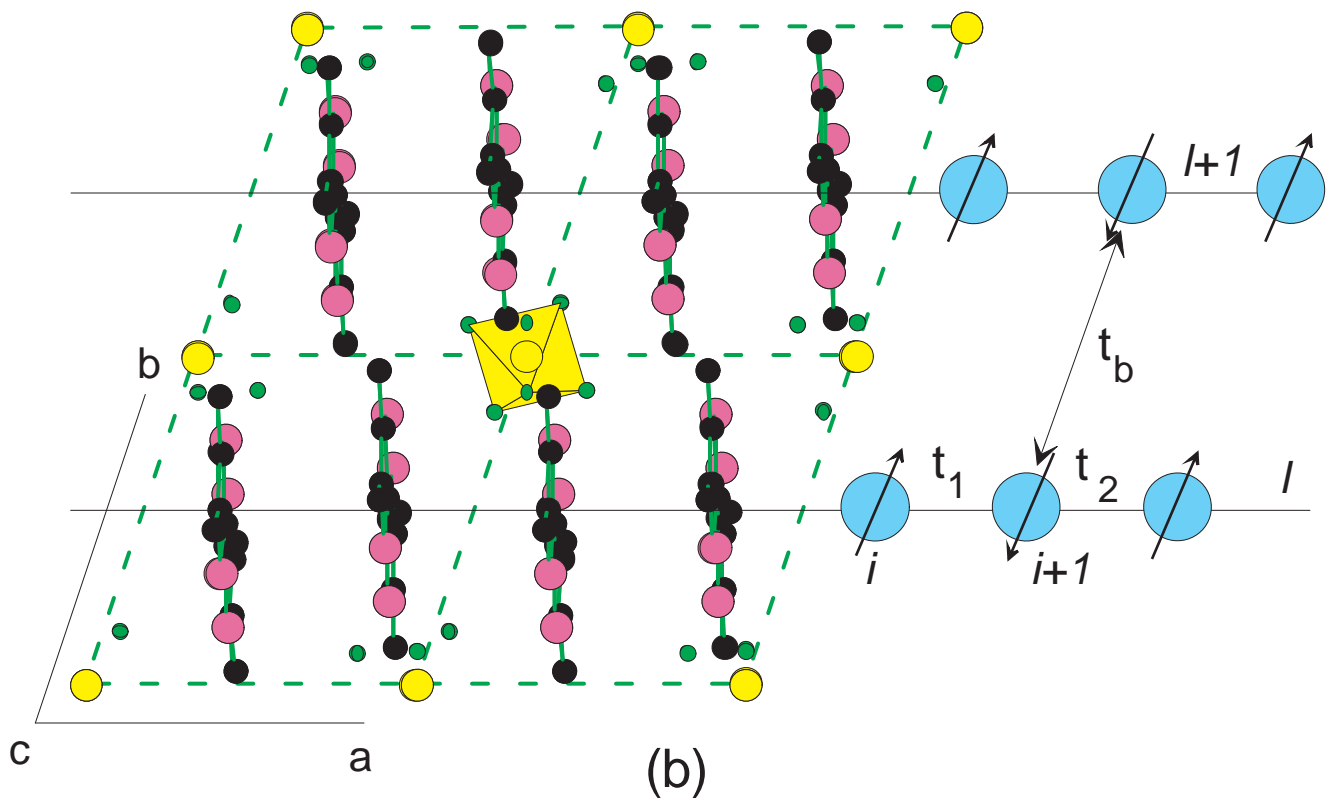
TABLE I: Raman mode frequencies of TMTSF₂PF₆, TMTSF neutral molecule and TMTSF⁺. A_g are Raman active modes of the TMTSF molecule within D_{2h} symmetry.

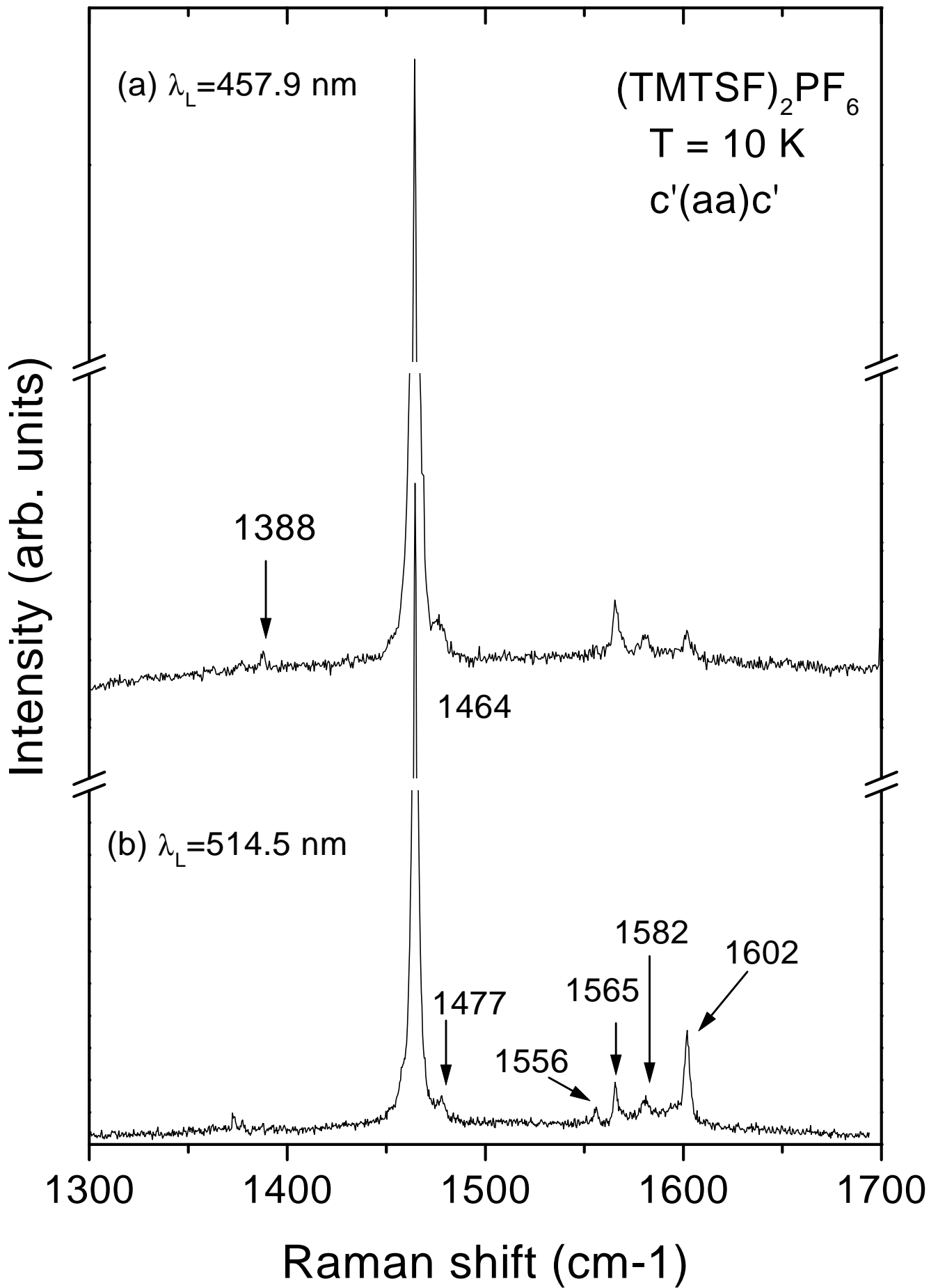
TMTSF ₂ PF ₆	TMTSF ₂ PF ₆	TMTSF ₂ PF ₆	TMTSF ⁰	TMTSF ⁺	A_g	Assignment
This work	Ref.[20]	Ref.[21]	Ref.[20]	Ref.[16]		Ref.[16]
156	-	155	173	-	ν_{12}	
181	-		-	180	-	
264	-	263	263	-	ν_{11}	CH ₃ - bending
284	278	281	276	285	ν_{10}	Se-Se stretching
-	-	-	-	317		-
331	-	328	328	-	-	
397	-	398	-	-	-	
452	-	452	453	452	ν_9	Se-C stretching
475	478	-	472	-	-	
-	-	-	603	-		
-	675	-	682	-	-	
916	917	918	916	924	ν_8	
921	-	-	-	-		
936	-	936	-	-		} C-C-H bending
-	1010	-	1018	-		
1071	-	1070	-	-	ν_7	
1092	-	-	-	-		
-	-	-	1167	-		
-	-	-	1225	1245		
1388	1381	-	1384	1386	ν_6	} H-C-H bending
1452	-	1452	1444	-	ν_5	
-	-	-	1503	-		
-	-	-	1530	-		
1464	1463	1464	1539	1399	ν_4	C=C in phase stretching
1477	-	1479	-	-		
1521	1547	-	-	-		
1565	1559	1565	1589	-		} H-C-H- bending
1582	-	1582	-	-		
1602	-	1601	1625	1573	ν_3	C=C out of phase stretching
2800	-	-	-	-	ν_2	C-H stretching
2908	2906	-	-	-	ν_1	C-H stretching

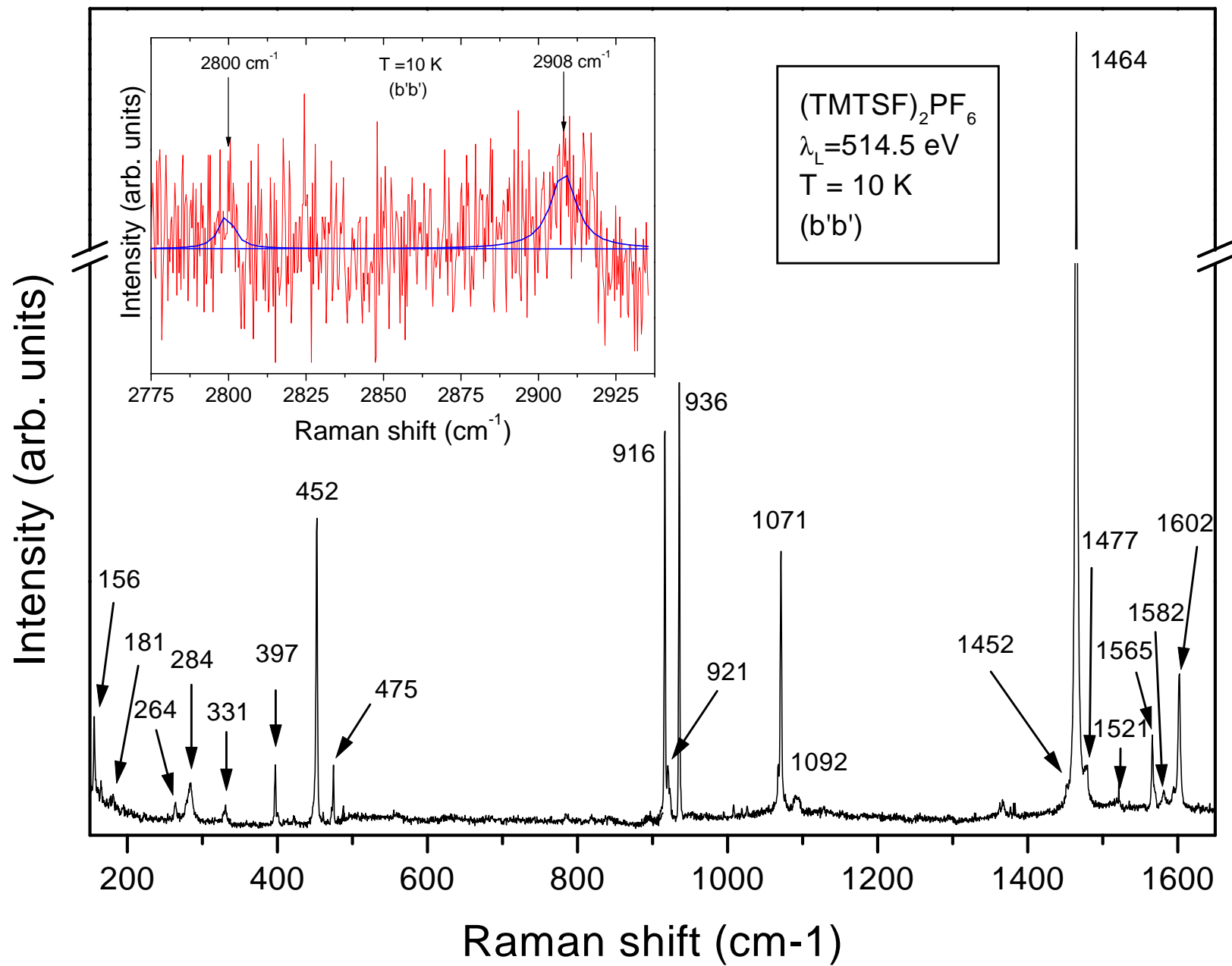


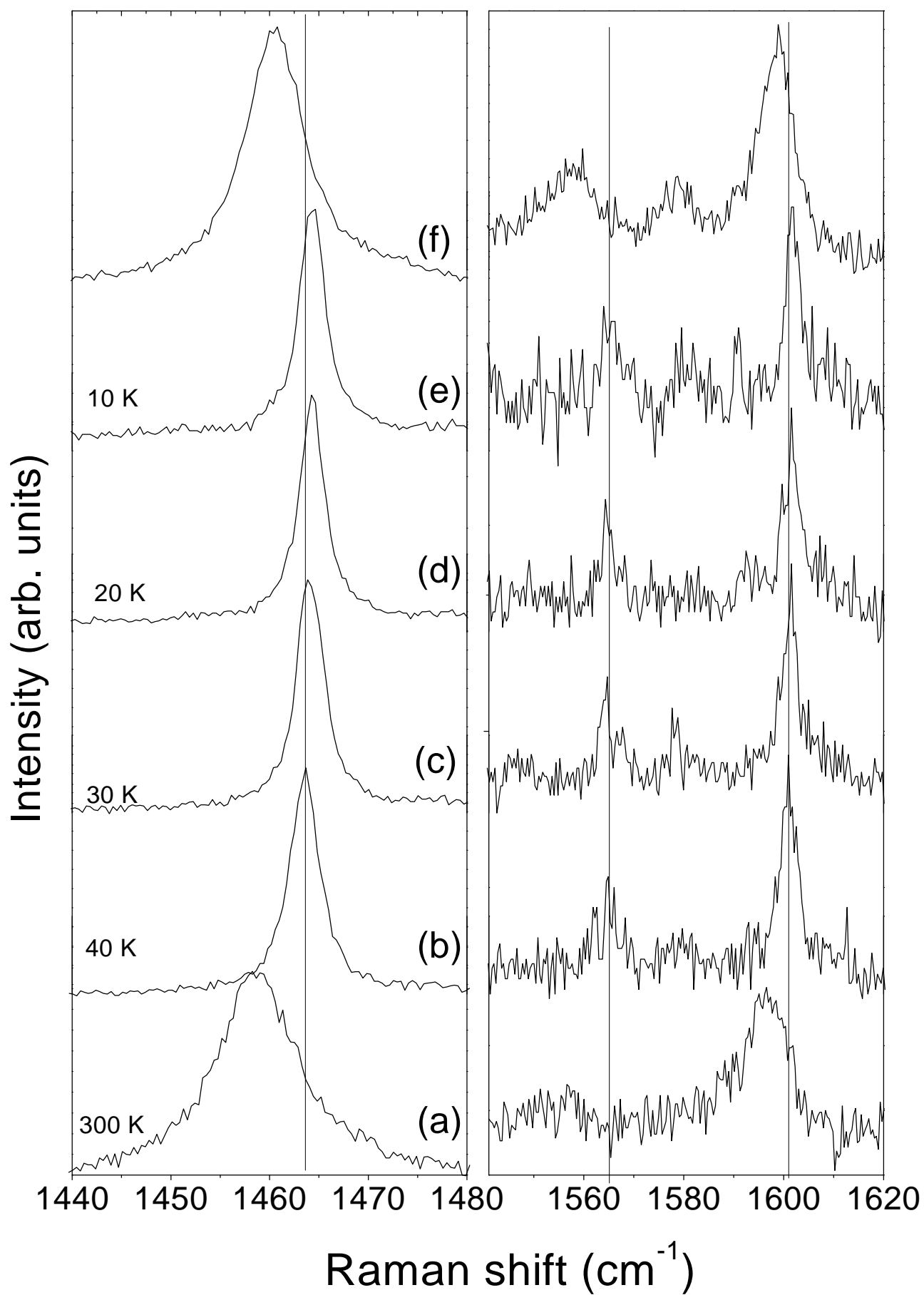
● C ● Se ● F ● P

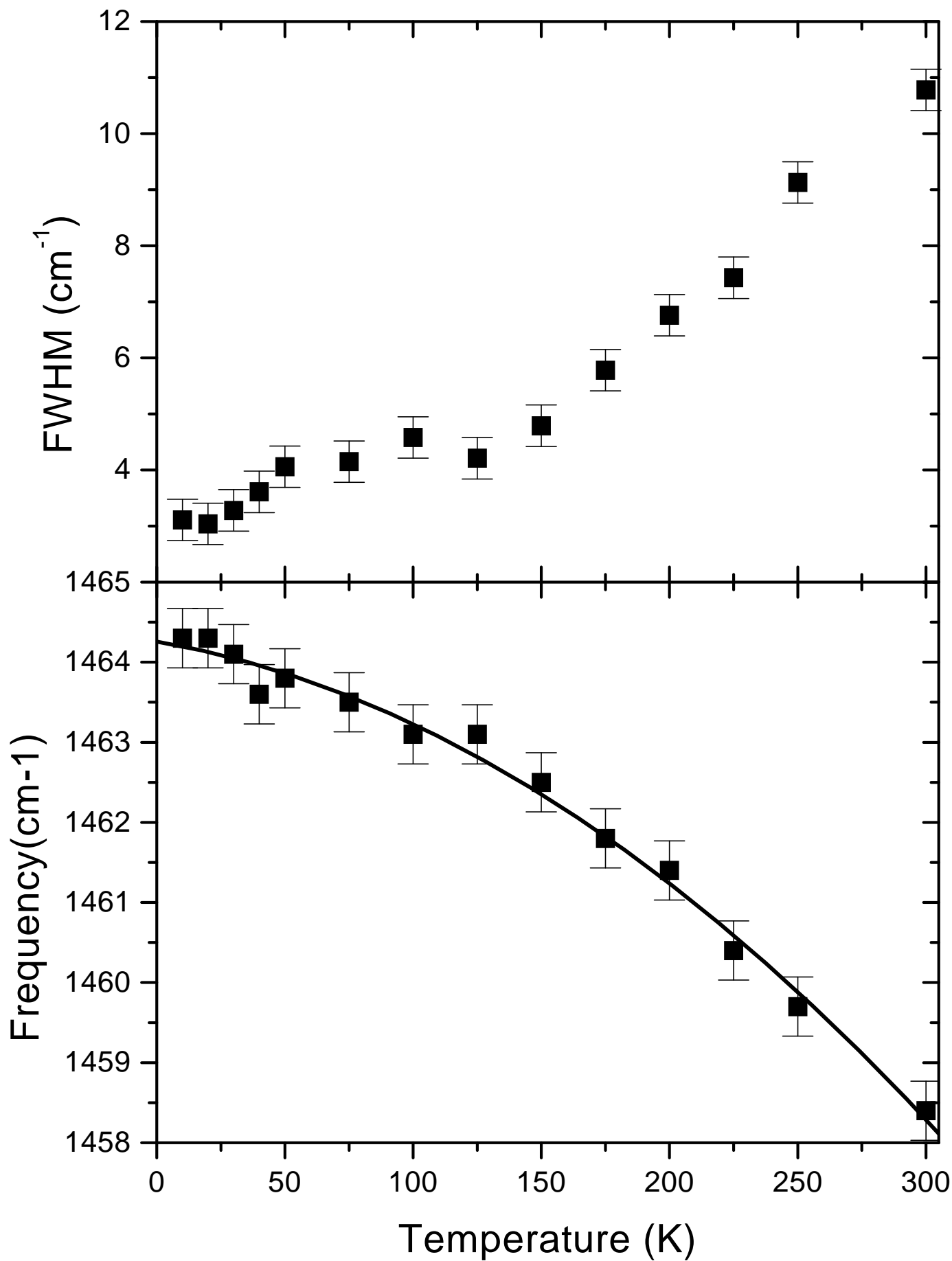
(a)

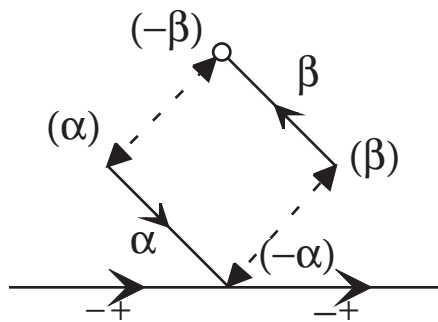
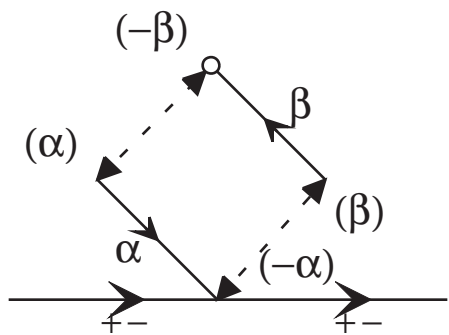




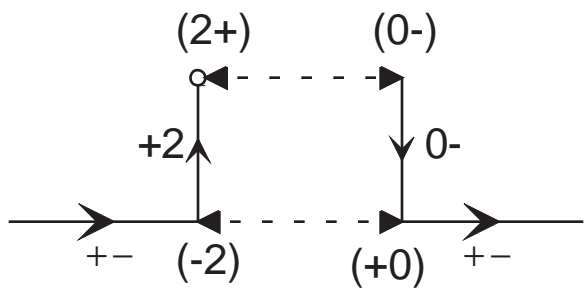




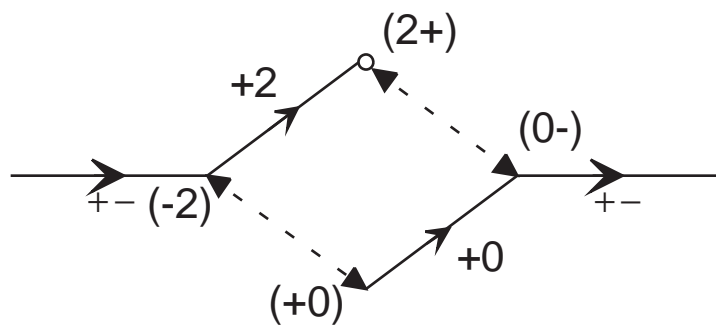




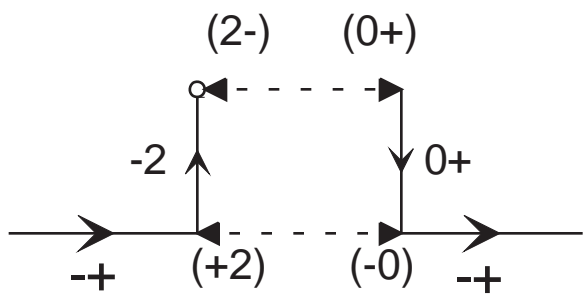
a)



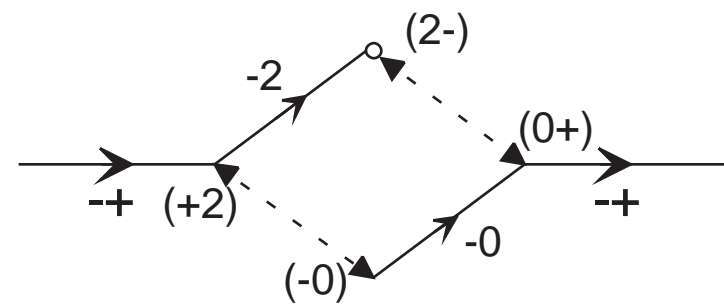
+



b)



+



c)